Nickel pincer model of the active site of lactate racemase involves ligand participation in hydride transfer

Tao Xu[a], Matthew D. Wodrich[a,b], Rosario Scopelliti[a], Clemence Corminboeuf[b], and Xile Hu[a,1]

[a]Laboratory of Inorganic Synthesis and Catalysis, Institute of Chemical Sciences and Engineering, Ecole Polytechnique Fédérale de Lausanne, Lausanne CH-1015, Switzerland; and [b]Laboratory for Computational Molecular Design, Institute of Chemical Sciences and Engineering, Ecole Polytechnique Fédérale de Lausanne, Lausanne CH-1015, Switzerland

Edited by David Milstein, The Weizmann Institute of Science, Rehovot, Israel, and accepted by Editorial Board Member Harry B. Gray December 19, 2016 (received for review September 27, 2016)

Lactate racemase is the first enzyme known to possess a metal pincer active site. The enzyme interconverts D- and L-lactic acid, which is important for the assembly of cell walls in many microorganisms. Here, we report a synthetic model of the active site of lactate racemase, which features a pyridinium-based SCS pincer ligand framework bound to nickel. The model complex mediates the dehydrogenation of alcohols, a reaction relevant to lactate racemization. Experimental and computational data indicate ligand participation in the dehydrogenation reaction.

biomimetic chemistry | lactate racemase | nickel | pincer ligands | hydride transfer

Pincer complexes are widely applied in homogeneous catalysis thanks to their stability, diversity, and tunability (1–4). However, only very recently has the first pincer complex been discovered in the active site of a metalloenzyme (5–7). It was reported that lactate racemase, an enzyme responsible for the racemization of lactic acid and hence important for cell wall assembly in many microorganisms, hosts a nickel pincer cofactor (Fig. 1). The nickel center is coordinated by an SCS pincer ligand derived from a nicotinic acid mononucleotide, in addition to histidine (200) (5, 6). Based on the structure of this active site, it was proposed that the pincer ligand could reversibly capture a hydride from lactate at the carbon atom coordinated to nickel, in a manner similar to nicotinamide adenine dinucleotide in hydride transfer enzymes (Fig. 1). Nevertheless, evidence for this mechanism is still lacking.

Although several nickel SCS pincer complexes have previously been reported (8–10), none exhibited an essential feature present in the active site of lactate racemase, namely a pyridinium-based pincer backbone. According to the proposed enzyme mechanism, the pyridinium group enables ligand participation in the hydride transfer reaction, which is likely impossible for a more conventional pyridine group. This hypothesis might be tested using model complexes containing either a pyridinium or a pyridine backbone. A further motivation for synthetic models of this unusual active site is the perspective of developing a new, bioinspired pincer ligand platform that enables metal ligand cooperation in catalysis (11, 12). With these considerations in mind, we began investigating the biomimetic chemistry of lactate racemase. Here, we report the synthesis and characterization of a synthetic mimic of lactate racemase. Using dehydrogenation of alcohols as a model reaction, we show that the pyridinium functionality indeed facilitates hydride transfer by ligand participation.

Results

Synthesis. The pyridine-based ligand precursor (**4**) was synthesized from 4-chloro-3,5-dimethyl pyridine (**1**, Fig. 2). Oxidation of **1** by $KMnO_4$ gave 4-chloropyridine-3,5-dicarboxylic acid (**2**), which was converted to a dicarboxamide (**3**) by amidation. Reaction of **3** with Lawesson's reagent [2,4-bis(4-methoxyphenyl)-2,4-dithioxo-1,3,2,4-dithiadiphosphetane] yielded the ligand precursor **4** containing thioamides (13). Upon treatment of **4** with $Ni(cod)_2$ (cod = 1,5-cyclooctadiene), a pyridine-derived nickel pincer complex **5** was formed. Attempts to alkylate the pyridine nitrogen of **5** by reaction with CH_3I or CH_3OTf (OTf = triflate) were unsuccessful. However, the reaction of **4** with CH_3I gave the pyridinium-derived ligand precursor **6**, which upon reaction with $Ni(cod)_2$, gave the pyridinium-derived nickel pincer complex **7**.

Characterization. In the UV-vis spectra, complex **5** exhibits an absorption peak at 450 nm, whereas complex **7** exhibits two absorption peaks at 365 and 456 nm (*SI Appendix*, Fig. S1). All these absorption peaks have an extinction coefficient of about 2,000 L $mol^{-1}\cdot cm^{-1}$. The pyridine pincer ligand **4** has only a very weak absorption peak at 380 nm, whereas the pyridinium pincer ligand has a strong absorption peak at 395 nm, with an extinction coefficient of about 2,000 L $mol^{-1}\cdot cm^{-1}$ as well (*SI Appendix*, Fig. S1). The spectrum of **7**, but not **4**-**6**, resembles that of lactate racemase, which exhibits two strong absorption peaks at about 380 and 450 nm (5). The spectra of **4**-**7** suggest that the absorption at about 380 nm is due to the pyridinium moiety, whereas the absorption at about 450 nm is due to the nickel ion.

Both complexes **5** and **7** are diamagnetic and can be characterized by conventional NMR spectroscopy (*SI Appendix*). The solid-state molecular structures of **5** and **7** were determined by X-ray crystallography, which confirmed the SCS pincer coordination mode (Fig. 3). In both complexes, the nickel center is in a square-planar geometry, with a Cl^- occupying the fourth coordination site. Upon methylation of the pyridine nitrogen, the

Significance

Pincer complexes are widely applied in homogeneous catalysis. However, only very recently has the first pincer complex been discovered in the active site of a metalloenzyme, namely, lactate racemase. Here, we report a synthetic model of the active site of lactate racemase. The nickel pincer model not only reproduces some key structural features of the active site, but also mediates the dehydrogenation of alcohols, a reaction relevant to lactate racemization. Our work suggests a mechanism in which the unique pyridinium-derived SCS pincer ligand actively participates in the hydride transfer. This work not only represents a successful biomimetic study of this enzyme but also lays the foundation for the development of new bioinspired pincer ligands.

Author contributions: T.X. and X.H. designed research; T.X. and M.D.W. performed research; R.S. and C.C. contributed analytic tools; T.X., M.D.W., R.S., C.C., and X.H. analyzed data; and T.X., M.D.W., and X.H. wrote the paper.

The authors declare no conflict of interest.

This article is a PNAS Direct Submission. D.M. is a Guest Editor invited by the Editorial Board.

Data deposition: The atomic coordinates and structure factors have been deposited in the Cambridge Structural Database, Cambridge Crystallographic Data Centre, www.ccdc.cam.ac.uk (accession codes: CCDC-1486993 and CCDC-1486994).

[1]To whom correspondence should be addressed. Email: xile.hu@epfl.ch.

This article contains supporting information online at www.pnas.org/lookup/suppl/doi:10.1073/pnas.1616038114/-/DCSupplemental.

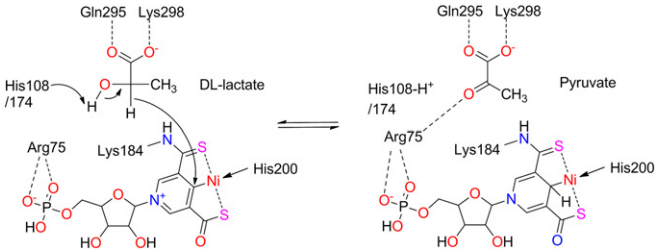

Fig. 1. Proposed catalytic mechanism of lactate racemase.

nickel–ligand bonds contract by only 0.02–0.03 Å while maintaining a nearly identical overall structure (Table 1). There is a lack of clear bond-length alteration within the pyridinium ring. The I^- anion sits above the positively charged N^+. These structural data indicate that the pincer backbone is best described by the 1-methyl pyridinium resonance form, as shown in Fig. 2, rather than the 1-methyl-pyridin-4-ylidene resonance form.

Density-functional theory (DFT) computations were performed to compare and contrast the electronic arrangement within complexes **5** and **7**. As evident from the computed Hirshfeld-I (14–16) and Mulliken (17) atomic charges (*SI Appendix*, Figs. S2 and S3), the positive charge of **7** is essentially located around the pyridinium nitrogen atom and in the SNiS region (*SI Appendix*, Fig. S2*B*). In contrast, the frontier orbitals (*SI Appendix*, Fig. S2 *C–F*), as well as the overall chemical bonding patterns of **5** and **7**, remain essentially identical [as illustrated by the density overlap regions indicator (DORI) (18) maps in *SI Appendix*, Figs. S4 and S5]. Thus, DFT analysis of the density and molecular orbitals [M06 (19, 20) /def2-SVP level] reveals no striking difference between the two pincer complexes. The DORI map of **7** (*SI Appendix*, Fig. S5*B*) shows no significant bonding differences between the C2–C3 and C3–C4 bonds, again consistent with the pyridinium formulation of the pincer backbone.

Dehydrogenation Activity. Lactate racemase is specific to lactic acid, and the proposed mechanism in Fig. 1 provides a possible explanation for this specificity. Upon binding to the active site, ion pairs involving lactate and ribose-5-phosphoric acid are formed. The lactate is stabilized by Glutamine (295) and Lysine (298), and Histidine (108/174) is involved in deprotonation of lactate. Thus, the second- and outer-sphere environment of the active site in the protein seems essential for enzyme activity. Consistent with this hypothesis, model complex **7** was inactive toward lactic acid and lactate. Considering that the possible role of the nickel active site is to mediate the hydride transfer reaction from an alcohol (lactate in the native case), we thought

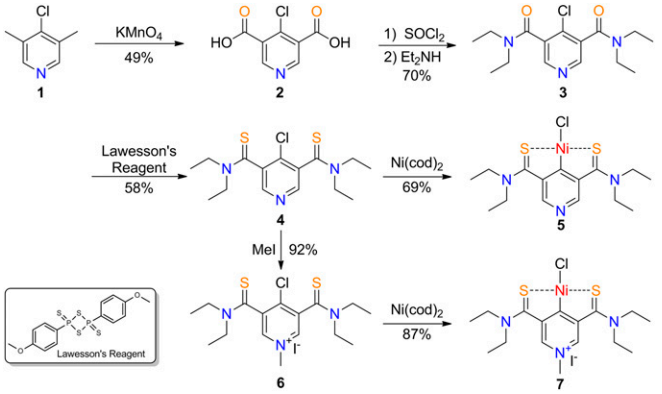

Fig. 2. Synthesis of the pincer ligands and complexes.

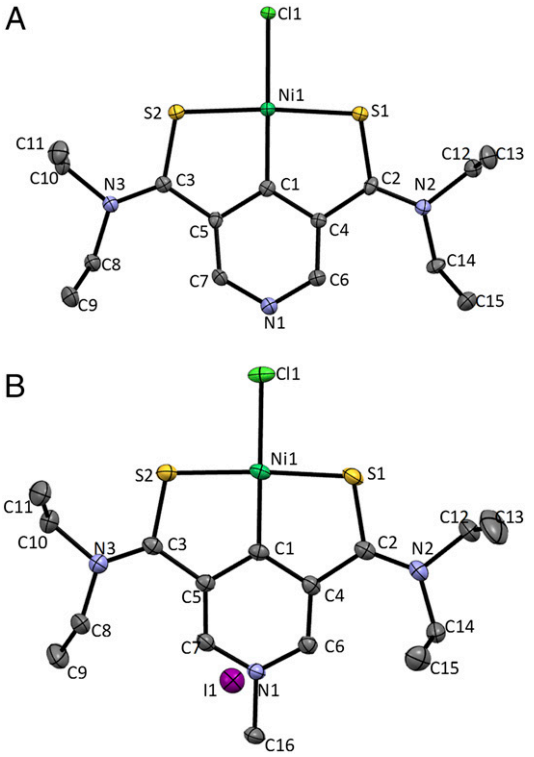

Fig. 3. Solid-state structure of complexes **5** (*A*) and **7** (*B*). The thermal ellipsoids are displayed at 50% probability.

dehydrogenation of alcohols would serve as a model reaction for enzyme activity. Thus, the activity of **7** for alcohol dehydrogenation was explored. It was found that **7** mediated the dehydrogenation of several primary and secondary alcohols (Fig. 4; for details, see *SI Appendix*, Table S1). For the dehydrogenation of benzyl alcohol (**8**), the best result involved equal amounts of **7**, benzyl alcohol, and (1,8-diazabicyclo[5.4.0]undec-7-ene), where benzaldehyde was obtained in a yield of 64%. It was found that **7** decomposed during the reaction, and no defined nickel species could be detected. However, under the standard condition, the protonated SCS ligand of **7** was observed in a 21% yield (**10**). Attempts to metallate **10** by reaction with $Ni(cod)_2$ were unsuccessful. When benzyl alcohol-α,α-D_2 (D_2-**8**) was used as the starting alcohol, deuterated D-**10** was found (*SI Appendix*, Fig. S6). As **7** mediated dehydrogenation of secondary alcohols, (*S*)-1-phenylethanol was used as probe for racemization. The dehydrogenation product acetophenone was obtained in a 49% yield, but no racemization of (*S*)-1-phenylethanol was detected

Table 1. Selected bond lengths and angles of complexes 5 and 7

Bond lengths, Å or angles, °	Complex **5**	Complex **7**
Ni–Cl	2.2585(11)	2.2287(9)
Ni–S1	2.1724(11)	2.1351(10)
Ni–S2	2.1707(11)	2.1427(9)
Ni–C1	1.862(4)	1.842(3)
S1–C2	1.717(4)	1.718(3)
S2–C3	1.726(4)	1.709(3)
S1–Ni–Cl	92.70(4)	91.92(4)
S1–Ni–S2	172.29(5)	176.36(4)
S1–Ni–C1	87.48(12)	87.96(10)
S2–Ni–Cl	92.14(4)	91.71(4)
Ni–S1–C2	101.78(14)	102.20(11)
Ni–S2–C3	101.63(14)	101.49(11)

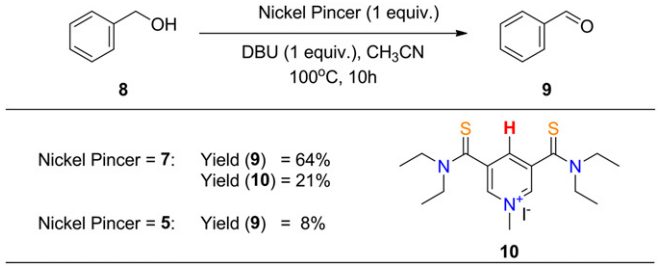

Fig. 4. Alcohol oxidation mediated by Ni pincer complexes. The reactions were conducted under N_2, and the yields were determined by GC using *n*-decane as the internal standard.

(*SI Appendix*, Table S1). When complex **5** was used in place of **7** as the mediator, the yield of dehydrogenation was close to baseline. The low yields obtained using complex **5** might be due to unidentified species formed upon decomposition of **5** during the reaction; the yields are similar to that obtained using $NiCl_2$. No dehydrogenation occurred when ligands **4** and **6** were used as the mediator, indicating the necessity of nickel for the reaction.

DFT Mechanistic Study. The significantly different activity of **7** and **5** in alcohol dehydrogenation suggests an important role of the pyridinium group in hydride transfer, which is mechanistically relevant to lactate racemase. DFT computations were conducted to probe the mechanism of alcohol dehydrogenation mediated by **7** and **5** (Figs. 5 and 6 and *SI Appendix*, Figs. S7–S9). Two mechanistic pathways were considered. The first pathway involves the formation of a nickel alkoxide complex from **7** (Fig. 5, $\mathbf{13_A}$), followed by β-H elimination ($\mathbf{13_{A'}}$) to form aldehyde (**9**) and a nickel hydride ($\mathbf{13_B}$). C-H reductive elimination of $\mathbf{13_B}$ would lead to formation of **10** along with an unligated nickel(0) species. However, this pathway is energetically inaccessible and would require overcoming a transition-state barrier associated with β-H elimination of greater than 40 kcal/mol (Fig. 6, blue pathways). A similar result was obtained for dehydrogenation mediated by complex **5** (Fig. 6 and *SI Appendix*, Fig. S8).

A second set of pathways involves either the C2 or C4 atom of the pyridinium and pyridine group acting as a hydride acceptor. In the case of **7**, the alcohol first associates with the nickel complex to give either reaction complex $\mathbf{11_A}$ or $\mathbf{12_A}$ (corresponding to C2 or C4 addition, respectively; Fig. 5). Deprotonation of the alcohol by a base and simultaneous hydride transfer from the α-carbon then gives the aldehyde product ($\mathbf{11_B}/\mathbf{12_B} + \mathbf{9}$). The computed free-energy

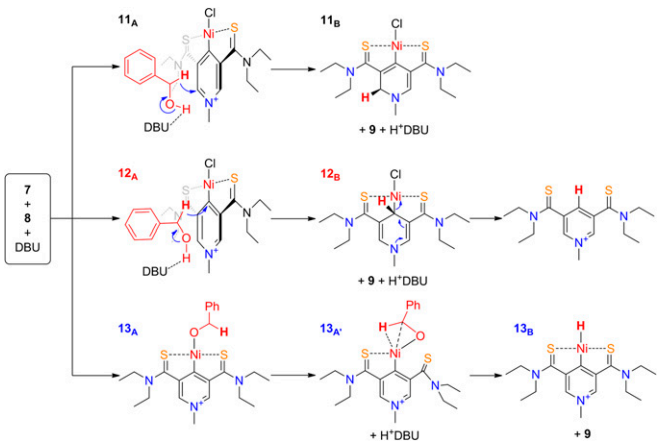

Fig. 5. Potential mechanisms for the dehydrogenation of benzyl alcohol mediated by complex **7**.

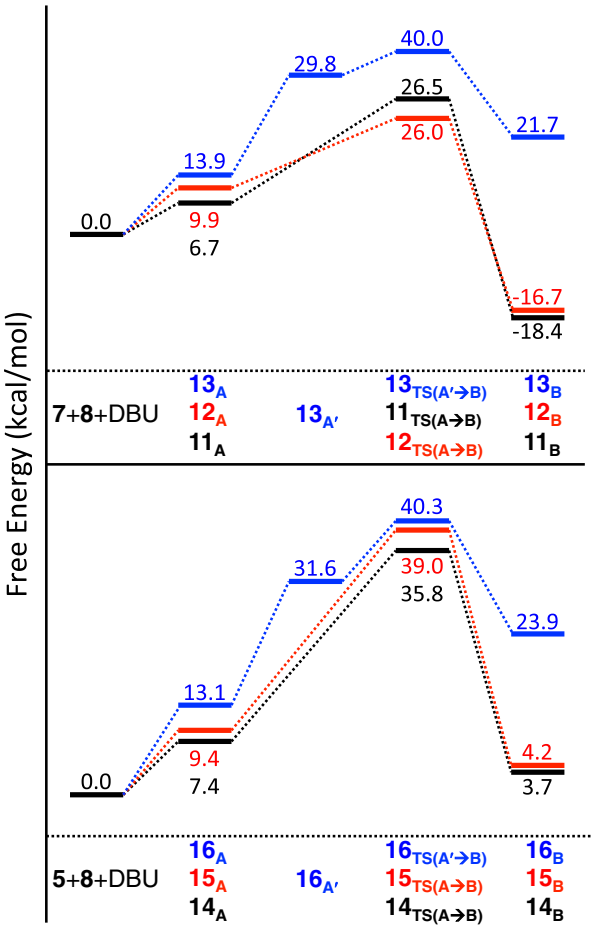

Fig. 6. Computed Gibbs free-energy profiles of possible mechanistic pathway for alcohol dehydrogenations by **7** and **5**. Reported free energies, in kilocalorie per mole, computed at the PBE0-dDsC/TZ2P//M06/def2-SVP level including solvation corrections in acetonitrile.

profiles [PBE0 (21, 22) –dDsC (23–26) /TZ2P//M06/def2-SVP level in implicit acetonitrile solvent COSMO-RS (27)]; see *SI Appendix* for full computational details] suggest that additions to C2 and C4 are roughly equally probable, as evidenced by nearly equivalent relative free energies for both the reaction complex ($\mathbf{11_A}/\mathbf{12_A}$) and the transition-state barriers corresponding to hydride addition ($\mathbf{11_{TSA\rightarrow B}}$,$\mathbf{12_{TSA\rightarrow B}}$). However, $\mathbf{12_B}$ is unstable with respect to rearomatization of the pyridinium group (11, 12), resulting in a demetallation from nickel that serves as a thermodynamic driving force for hydride addition to C4. In contrast to $\mathbf{12_B}$, compound $\mathbf{11_B}$ is unable to follow a rearomatization pathway. However, the presence of $\mathbf{11_B}$ as an intermediate cannot be ruled out entirely, as a relatively low-energy isomerization pathway that facilitates the interconversion of $\mathbf{12_B}$ and $\mathbf{11_B}$ may exist. Preliminary DFT computations point to a hydrogen transfer network involving the use of multiple hydrogen-bonded alcohol molecules, as the direct cross-ring transfer was found to be very energetically unfavorable (i.e., >60 kcal/mol).

Whereas similar pathways exist for both **5** and **7**, the overall computed free-energy profile (Fig. 6) clearly supports the experimentally observed enhanced reactivity of **7** over **5**. Aside from having an overall reaction energy that is endergonic, aldehyde formation by **5** that is achieved via hydride transfer to either the C2 or C4 of the pyridine is associated with significantly higher transition-state barrier heights than the corresponding hydride additions to the pyridinium ring in **7** (~36 kcal/mol vs. ~26 kcal/mol). Moreover, aldehyde formation by **7** is associated

with an overall exergonic free energy (~−17 kcal/mol), whereas its formation by **5** is endergonic (~4 kcal/mol). Thus, DFT computations confirm the ligand-centered reaction pathway for dehydrogenation and the essential role of the pyridinium pincer ligand.

Discussion

The alcohol dehydrogenation catalyzed by lactate racemase is reversible, leading to lactate racemization. The alcohol dehydrogenation mediated by complex **7** is irreversible, presumably due to the demetallation of the nickel-containing intermediate after hydride transfer. The histidine (200) ligand, as well as the protein environment, might contribute to the higher stability of the enzyme intermediate compared with its synthetic analog. Moreover, there are still substantial differences between the coordination environment of the enzyme active site and that of complex **7**. The two sulfur donors in the enzyme are asymmetric, whereas in **7** they are symmetric. Whereas both the active site and **7** have two neutral and two anionic ligands, the anionic ligands in the active site are in a *cis*,*cis* arrangement, while their counterparts in **7** are in a *trans*,*trans* arrangement. These differences may influence the reactivity of the complexes and alter the tendency for the pincer ligands to undergo demetallation. Further tuning of the ligand environment is needed to produce a more faithful mimic, to stabilize the synthetic intermediate, and to turn the dehydrogenation reaction catalytic. Despite these limitations, the current work is an important step in the biomimetic chemistry of lactate racemase. The drastic reactivity difference between **5** and **7** and the DFT computations provide insights into the enzyme reaction mechanism. Additionally, the pyridinium-based pincer SCS ligand developed here is new in molecular chemistry (28, 29) and may find novel applications in coordination chemistry and homogeneous catalysis.

Conclusion

In conclusion, we report a small-molecule model of the active site of lactate racemase. This nickel pincer model not only reproduces some essential structural features of the active site, but also mediates alcohol dehydrogenation, a key step in enzyme activity. Experimental and DFT data support a mechanism in which the pyridinium SCS pincer ligand acts as a hydride acceptor in alcohol dehydrogenation. This result will inspire the design of new bio-inspired pincer ligands, which can engage in metal–ligand cooperative catalysis. Further work will also focus on the stabilization of reaction intermediates and improvement of reactivity.

Materials and Methods

See *SI Appendix* for details of materials and methods: UV-vis (*SI Appendix*, Fig. S1), NMR (*SI Appendix*, Figs. S6, S12–21), and FTIR spectra (*SI Appendix*, Figs. S10 and S11), as well as DFT computational results (*SI Appendix*, Figs. S2–S5 and S7–S9). See Datasets S1 and S2 for crystallographic data.

ACKNOWLEDGMENTS. This work is supported by the Swiss National Science Foundation (Grant 200020_152850/1) and the Ecole Polytechnique Fédérale de Lausanne.

1. Szabo KJ, Wendt OF (2014) *Pincer and Pincer-Type Complexes* (Wiley-VCH, Weinheim).
2. Morales-Morales D, Jensen CM (2007) *The Chemistry of Pincer Compounds* (Elsevier, Amsterdam).
3. Albrecht M, van Koten G (2001) Platinum Group Organometallics Based on "Pincer" Complexes: Sensors, Switches, and Catalysts. *Angew Chem Int Ed Engl* 40(20):3750–3781.
4. van der Boom ME, Milstein D (2003) Cyclometalated phosphine-based pincer complexes: Mechanistic insight in catalysis, coordination, and bond activation. *Chem Rev* 103(5):1759–1792.
5. Desguin B, et al. (2015) A tethered niacin-derived pincer complex with a nickel-carbon bond in lactate racemase. *Science* 349(6243):66–69.
6. Desguin B, Soumillion P, Hols P, Hausinger RP (2016) Nickel-pincer cofactor biosynthesis involves LarB-catalyzed pyridinium carboxylation and LarE-dependent sacrificial sulfur insertion. *Proc Natl Acad Sci USA* 113(20):5598–5603.
7. Xu T, Bauer G, Hu X (2016) A novel nickel pincer complex in the active site of lactate racemase. *ChemBioChem* 17(1):31–32.
8. Kruithof CA, et al. (2008) X-ray and NMR study of the structural features of SCS-pincer metal complexes of the Group 10 triad. *Organometallics* 27(19):4928–4937.
9. Peterson SM, Helm ML, Appel AM (2015) Nickel complexes of a binucleating ligand derived from an SCS pincer. *Dalton Trans* 44(2):747–752.
10. Koizumi Y, et al. (2010) Nickel(II) complexes bearing a pincer ligand containing thioamide units: Comparison between SNS- and SCS-pincer ligands. *Inorg Chim Acta* 363(11):2474–2480.
11. Khusnutdinova JR, Milstein D (2015) Metal-ligand cooperation. *Angew Chem Int Ed Engl* 54(42):12236–12273.
12. Gunanathan C, Milstein D (2011) Metal-ligand cooperation by aromatization-dearomatization: A new paradigm in bond activation and "green" catalysis. *Acc Chem Res* 44(8):588–602.
13. Hossain MA, Lucarini S, Powell D, Bowman-James K (2004) Ditopic double pincer palladacycle catalyst for C-C coupling. *Inorg Chem* 43(23):7275–7277.
14. Hirshfeld FL (1977) Bonded-atom fragments for describing molecular charge densities. *Theor Chim Acta* 44(2):129–138.
15. Bultinck P, Van Alsenoy C, Ayers PW, Carbó-Dorca R (2007) Critical analysis and extension of the Hirshfeld atoms in molecules. *J Chem Phys* 126(14):144111.
16. Gonthier JF, Steinmann SN, Wodrich MD, Corminboeuf C (2012) Quantification of ''fuzzy'' chemical concepts: a computational perspective. *Chem Soc Rev* 41:4671–4687.
17. Mulliken RS (1955) Electronic population analysis on LCAO–MO molecular wave functions. *J Chem Phys* 23:1833.
18. de Silva P, Corminboeuf C (2014) Simultaneous visualization of covalent and noncovalent interactions using regions of density overlap. *J Chem Theory Comput* 10(9): 3745–3756.
19. Zhao Y, Truhlar DG (2008) Density functionals with broad applicability in chemistry. *Acc Chem Res* 41(2):157–167.
20. Zhao Y, Truhlar DG (2008) The M06 suite of density functionals for main group thermochemistry, thermochemical kinetics, noncovalent interactions, excited states, and transition elements: Two new functionals and systematic testing of four M06-class functionals and 12 other functionals. *Theor Chem Acc* 120(1):215–241.
21. Perdew JP, Burke K, Ernzerhof M (1996) Generalized gradient approximation made simple. *Phys Rev Lett* 77(18):3865–3868.
22. Adamo C, Barone V (1999) Toward reliable density functional methods without adjustable parameters: The PBE0 model. *J Chem Phys* 110:6158.
23. Steinmann SN, Corminboeuf C (2010) A system-dependent density-based dispersion correction. *J Chem Theory Comput* 6(7):1990–2001.
24. Steinmann SN, Corminboeuf C (2011) A density dependent dispersion correction. *Chimia (Aarau)* 65(4):240–244.
25. Steinmann SN, Corminboeuf C (2011) A generalized-gradient approximation exchange hole model for dispersion coefficients. *J Chem Phys* 134(4):044117.
26. Steinmann SN, Corminboeuf C (2011) Comprehensive benchmarking of a density-dependent dispersion correction. *J Chem Theory Comput* 7(11):3567–3577.
27. Klamt A (2011) The COSMO and COSMO-RS solvation models. *WIREs Comput Mol Sci* 1(5):699–709.
28. Horak KT, VanderVelde DG, Agapie T (2015) Tuning of metal complex electronics and reactivity by remote Lewis acid binding to Π–coordinated pyridine diphosphine ligands. *Organometallics* 34(19):4753–4765.
29. Meguro H, Koizumi TA, Yamamoto T, Kanbara T (2008) Synthesis, structure, and quaternization and complexation reactions of $_{\kappa}{}^{3}$SCS pincer palladium complexes having 3,5-pyridinediyl unit. *J Organomet Chem* 693:1109–1116.